A positron-annihilation study of the electronic structure of CeB_6

1994 J. Phys.: Condens. Matter 6 7823

(http://iopscience.iop.org/0953-8984/6/38/019)

J. Phys.: Condens. Matter 6 (1994) 7823–7831. Printed in the UK

A positron-annihilation study of the electronic structure of CeB_6

M Biasini†¶, M A Alam‡, H Harima‡*, Y Onuki§, H M Fretwell‡ and R N West‖

† ENEA, Viale Ercolani 8, 40138 Bologna, Italy
‡ H H Wills Physics Laboratory, University of Bristol, Tyndall Avenue, Bristol BS8 1TL, UK
§ Institute of Material Science, University of Tsukuba, Tsukuba, Ibaraki 305, Japan
‖ University of Texas at Arlington, Arlington, TX 76019, USA

Abstract. The two-dimensional angular correlation of electron–positron annihilation radiation (2D ACAR) from the heavy-fermion dense Kondo system CeB_6 was measured. The anisotropies of the measured momentum spectra were in reasonable agreement with those of model spectra based on the Fermi-surface topology suggested by band-structure calculations and de Haas–van Alphen measurements. However, the related k-space densities, obtained by an LCW analysis, were far removed from those expected from the Fermi-surface topology. The use of a recently developed filter procedure, designed to remove the characteristic long-range distortions that are frequently encountered in such LCW spectra, provided a much improved image of the Fermi-surface features.

1. Introduction

Among the rare-earth and actinide compounds, the rare-earth hexaborides RB_6 (R = La, Ce, Pr and Nd) display a variety of behaviours that have been ascribed to the different roles played by their f electrons. With an empty f shell LaB_6 is a paramagnetic metal (its electron effective mass is smaller than the free-electron mass), PrB_6 and NdB_6 are local moment magnetically ordered metals and CeB_6 is a typical Kondo-lattice heavy-fermion compound. The most recent de Haas–van Alphen (dHvA) measurements [1, 2] on CeB_6, which confirm that the features of its Fermi surface (FS) are similar to those of LaB_6, are consistent with a model of the FS in which the f-electron degree of freedom does not contribute to the Fermi volume.

In CeB_6 a very unusual magnetic phase diagram [3] gives rise to two ordering transitions: a quadrupolar ordering (phase II) at the temperature $T_q = 3.2$ K and an antiferromagnetic ordering (phase III) at the Néel temperature $T_N = 2.3$ K. As the dHvA measurements noted above were performed in phase II, they can be fruitfully complemented by a measurement of the two-dimensional-angular-correlation-of-positron annihilation-radiation (2D-ACAR) technique in the paramagnetic phase (I).

A 2D-ACAR experiment [4] determines a two-dimensional (2D) projection or integral, $N(p_x, p_y)$, of an underlying 3D electron–positron momentum distribution $\rho(\boldsymbol{p})$. The integration direction, p_z, specified by the main axis of the spectrometer, is usually along a major symmetry direction of the single-crystal specimen. $\rho(\boldsymbol{p})$ for a periodic solid is most easily described, in a one-electron approximation, as a superposition of contributions from

¶ Present address: H H Wills Physics Laboratory, University of Bristol, Tyndall Avenue, Bristol BS8 1TL, UK.
* Permanent address: CIAS, University of Osaka Prefecture, Sakai, Osaka 593, Japan.

0953-8984/94/387823+09$19.50

occupied states, of band index n and reduced Bloch wave vector k. Those contributions occur at various points, $p = \hbar(k + G)$, where G is a reciprocal lattice vector, with relative intensities determined by matrix elements involving electron and positron wave function products. The consequent, overall contribution from each band has the full point symmetry of the crystal lattice and an overall shape that reflects the nature (s, p, d; core or conduction etc) of the band in question. For a full band it is continuous. For a part-full band there are, in addition, discontinuities at all points $p_F = \hbar(k_F + G)$. The discontinuities mark the FS. 2D-ACAR measurements have yielded unique information concerning the FS and other aspects of the electronic structure of other even more complex compounds [5]. However, previous positron results for the rare-earth hexaborides [6,7] have shown some discrepancies with the results of theoretical calculations and with dHvA data.

In this paper the results of a new series of high-precision measurements are presented and analysed. Raw spectra of a very high level of statistical precision have been subjected to a traditional 2D-ACAR analysis supplemented by a new filter procedure that separates the FS signals from other structures in the spectra. It is shown that main features of the FS of CeB_6, as seen in the filtered data, confirm in great part the low-temperature quantum-oscillation measurements and are in good agreement with the theoretical calculations. To our knowledge this provides one of the first substantial evidences of the applicability of the positron-annihilation technique to the study of the FS topology in heavy-fermion systems.

2. Experimental details

The sample was a CeB_6 single crystal of dimensions 3.6 mm × 2.9 mm × 2.4 mm, which had displayed the typical Kondo effect in a separate resistivity measurement. The experiments were performed at a temperature of 30 K and a pressure of 10^{-6} Torr on a recently set up 2D-ACAR system [8] based on a pair of Anger cameras [9]. Each camera comprised a 42 cm diameter, 1.25 cm thick Na(I) crystal scintillator, optically coupled to a close-packed honeycomb array of 61 photomultipliers. The coincidence-timing resolution (for photon pair selection) was 60 ns. A 12 m sample–detector distance provided a coincidence angular field of view of 34.5×34.5 mrad^2 in a (256×256)-bin matrix. At this distance the estimated optical resolution of the system was 0.55 mrad or, equivalently, 0.075 atomic (momentum) units (au). This, with the intrinsic sizes of the positron source spot at the sample and the thermal spread of the positron, yielded an estimated overall resolution of (0.07, 0.1) au for the p_x and p_y directions respectively (9% and 12% of the BZ size).

We performed two measurements: the first, with integration along the [100] direction of the crystal, to a total $\sim 3.5 \times 10^8$ coincidence counts; the second, along [110], to 1.1×10^8 counts. At the completion of the measurements, the two 'raw' spectra were first corrected with the so-called momentum sampling function [9], which removes the distortions resulting from spatial variations in the single-detector efficiencies and the finite apertures of those detectors. Then the corrected spectra were examined for evidence that, within the limitations of the prevailing statistics and the already noted anisotropy in angular resolution, they reflected the appropriate projected crystal point symmetry (point group $4mm$). That being so, they were then folded along the directions p_x and p_y, to improve their effective precision.

3. Results and discussion

The unit cell of all the rare-earth hexaborides (RB_6) is simple cubic: it contains an R atom

and a regular octahedron of six B atoms. The R atoms and the B octahedra form two interpenetrating simple cubic crystal lattices.

Consistent with the latest dHvA measurements, recent band-structure calculations [10], based on local models where the 4f orbitals are treated like incompletely occupied core states, suggest an FS topology for CeB_6 similar to that of LaB_6. The latter consists of a set of nearly symmetrical, electron ellipsoids [11] centred at the X points and connected by thick necks along the Γ–M (Σ) axes (figure 1). The ellipsoids arise from a band having mainly La-5d character near the X points and B-2p character near the Γ point. In addition to this main FS sheet, a joint effort of theory and experiments [12] has established, in LaB_6, a second sheet of 12 smaller electron pockets along the Γ–M directions.

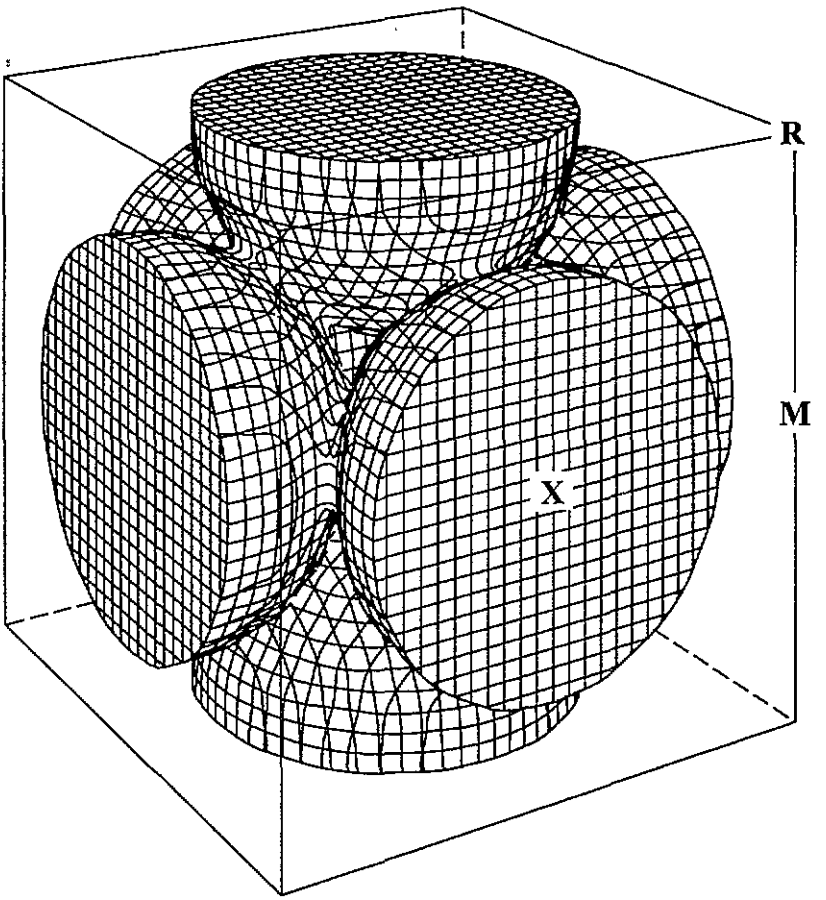

Figure 1. The multiply connected ellipsoidal FSs of CeB_6. The ellipsoid radii assumed were 34% and 39% of the BZ for the XM and ΓX directions respectively (after [2]).

This has allowed the solution of previous inconsistencies regarding the shape and sizes of the ellipsoid necks. Recent acoustic dHvA measurements [13] have detected frequencies corresponding to equivalent electron pockets in CeB_6 although they differ in size from those in LaB_6.

In figure 1 we show a CeB_6 FS model consisting of regular ellipsoids with sizes adopted from dHvA and acoustic dHvA measurements [2, 13]. Figures 2 and 3 show the k-space electron occupancies in the first Brillouin zone (BZ) obtained by integrating the model along the experimental projection directions and convoluting the results with the assumed resolution function. Contributions from electron pockets were not included; their action would be, however, to soften the flat-top character of the four 'mountains' between ΓXX and XMM in figure 2 (which arise from the ellipsoids' necks) and to distort the topology of the two main 'mountains' at XX in figure 3.

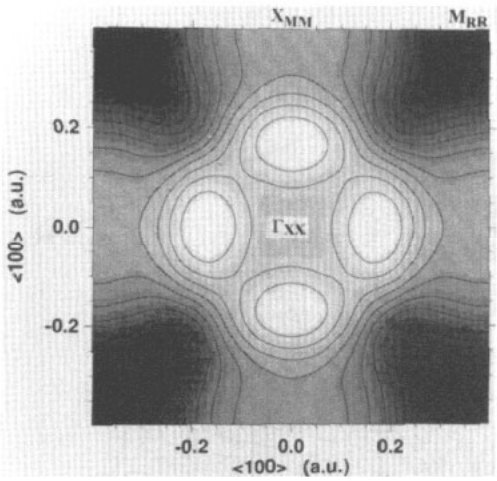

Figure 2. Electron occupancies in k space obtained by integrating the FS model of figure 1 along the [100] direction. The result was convoluted with a resolution function of 0.084 au corresponding to the average of the experimental resolutions along the two resolved momentum directions. The labelling describes the projected high-symmetry points. In this and all following figures, white corresponds to high and black to low.

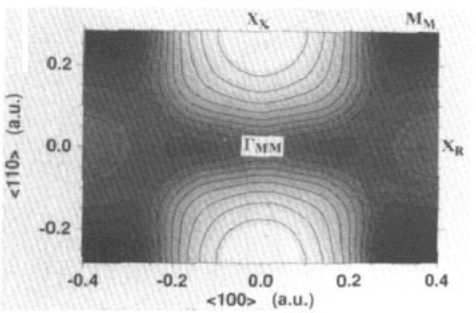

Figure 3. As figure 2 except that here the integral is along the [110] direction and has been convoluted with the asymmetric resolution of the spectrometer (see section 2).

Because a display of the 2D-ACAR data for a complex, multi-band system is seldom particularly illuminating, it has become common practice [5] to show the difference between the spectrum and its angular average. By this procedure one can eliminate the large isotropic part of the contribution originating from full valence bands and core electrons and focus on the anisotropies in the spectrum. The maximum magnitudes of the anisotropies in the twice-folded (with respect to the p_x and p_y axes) spectra for the [100] and [110] projections were 2.5% and 3.6% of the maximum, respectively. For better comparison with the theoretical calculations and to increase further the effective statistics, the already twice-folded [100] projection was folded again along the [110] symmetry (diagonal) axis. This removed the effect of the different resolution of the spectrometer along the x and y directions and restored the appropriate fourfold symmetry. Figures 4 and 5 show the resulting anisotropy parts of the thrice-folded [100] and twice-folded [110] projections.

In figure 4, the four minima at (2.9, 2.9) mrad reflect very well the lows in figure 2 at the corner of the projected Brillouin zone (MRR) expected from the FS model. Other features are in good agreement with those of the anisotropy of a simulated spectrum (figure 6). In this

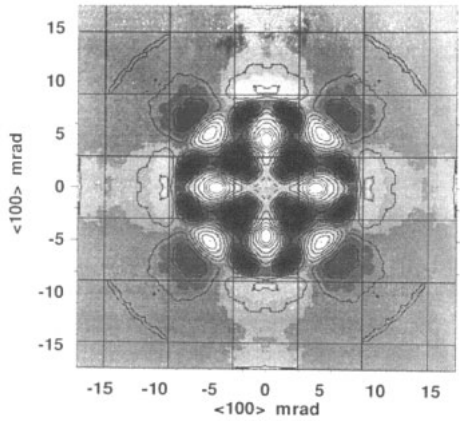

Figure 4. The anisotropy of the measured and symmetrized (see the text) momentum density for integration along the [100] direction. The spectrum was smoothed with an equally weighted smoothing array of 0.67×0.67 mrad^2 (1 mrad = 0.137 au). The borders of the projected first BZ in a repeated-zone scheme are shown.

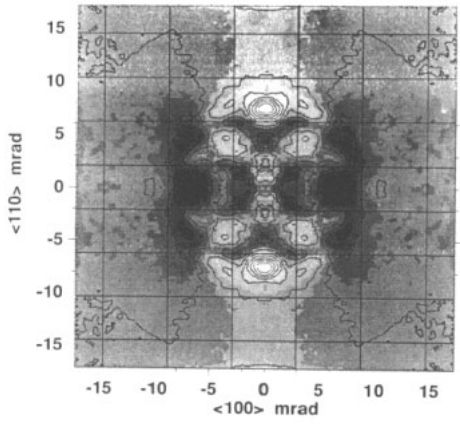

Figure 5. As figure 4 but for integration along the [110] direction. The borders of the projected first BZ in a repeated-zone scheme are shown.

model spectrum, the contribution of the conduction electrons was generated by modulating the appropriately projected electron occupancies (as defined by the FS model of figure 1) in a multiply repeated zone scheme, by a Gaussian obtained by a fit of the experimental data. A further Gaussian function represented the contribution from the filled bands. No provision was made for momentum wave-function anisotropies.

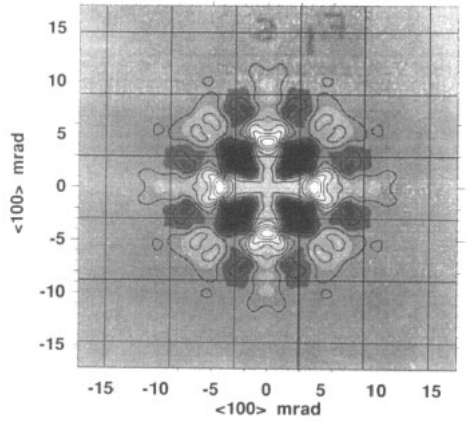

Figure 6. The anisotropy of the simulated spectrum for the [100] integration direction constructed as described in the text. The width of the modulation Gaussian adopted to approximate the reduction of the intensity at higher zones was taken from a fit of the experimental data (FWHM = 9.8 mrad). The borders of the projected first BZ in a repeated zone sheme are shown.

The model spectrum features both the observed lows at (2.9, 2.9) mrad and the maxima at (0, 4) and (4, 0) mrad. The further highs at (5, 5) mrad are less evident. Notwithstanding this, the overall correspondence with experiment is surprisingly good for the [100] projection. It was less so for the [110] projection. There, the observed highs at (0, 7.5) mrad and the lows at (7, 0) mrad are not consistent with higher-momentum images

of the FS and must be therefore merely consequences of electron wave-function momentum anisotropies. However, the topology of the anisotropy in the first BZ, with shallow minima at the centre of the distribution and at the corners of the zone, is not inconsistent with that of the projected FS (see figure 3).

In 2D-ACAR studies of metallic solids the FS is always a major preoccupation since it provides the most direct and transparent check of a theoretical band-structure calculation. Then, the so-called LCW [14] transformation often proves useful. In this transformation the measured momentum density is folded back into a primitive zone of the projected reciprocal lattice. In the transformed density, the FS structures that were originally distributed throughout the original momentum density, at points $\boldsymbol{p}_F = \hbar(\boldsymbol{k}_F + \boldsymbol{G})$, are brought together to form a set of coherent and reinforced images of the FS in the equivalent region of k space. The continuous parts of the original density, henceforth referred to as wave-function effects, sum into a large-intensity and relatively smooth background in which the only variations amount to a superposition of a few long-wavelength and small- (few % or so of the background) amplitude cosines. Figures 7 and 8 show the LCW-processed data for the [100] and [110] projections. The total amplitude variations are 3.3% and 2.4% for [100] and [110], respectively. The agreement with the theoretical data is certainly only partial and consists essentially in the lows at the corners of the BZ (points labelled MRR) in the [100] projection and in the lows at XMM and the saddle point at ΓMM in the [110] projection. The predicted low at ΓXX and surrounding four highs in the theoretical [100] projection (figure 2) are missing. As many features of the simulated anisotropy of the [100] projection were consistent with the anisotropy of the experimental data, one is forced to conclude (at least for the [100] projection) that the difference between the experimental and theoretical pictures is due to appreciable cosine amplitudes arising from the full-band contributions. As an initial test of this hypothesis we applied the LCW transformation to an isotropic approximation to the experimental momentum spectrum. This comprised two Gaussian components having a full width at half maximum (FWHM) of 9.8 mrad (35% intensity) and 6.74 mrad respectively. The results (not shown) were very similar to those of the experimental LCW for the [100] projection and had a total amplitude variation of 4.8%.

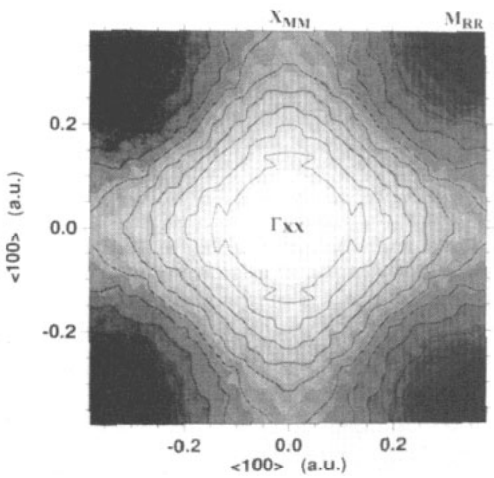

Figure 7. The experimental LCW k-space density: the integration direction is [100]. The BZ and symmetry point notation is as in figure 2.

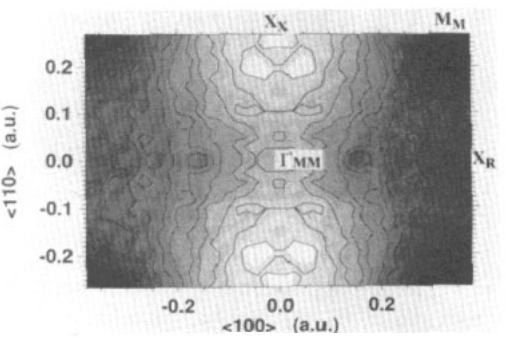

Figure 8. The experimental LCW k-space density: the integration direction is [110]. The BZ and symmetry point notation is as in figure 3.

In light of this an 'image enhancement technique' [15] was employed. Such techniques have been recently introduced into ACAR data analyses and their usefulness in FS studies has been well demonstrated elsewhere [16, 17]. In this work we adopted the simple and fast three-step procedure described in [16]. First, the spectrum to be filtered is smoothed (here with a simple (15 × 15)-channel unweighted mask). Then the smoothed spectrum is subtracted from the original. The result is a difference spectrum of much lower intensity from which almost all of the long-wavelength (in LCW, cosine) variations have been removed while the more rapidly varying FS discontinuities and statistical noise are enhanced. A final, light (three- or five-channel) smoothing is then applied to the difference spectrum to suppress the noise.

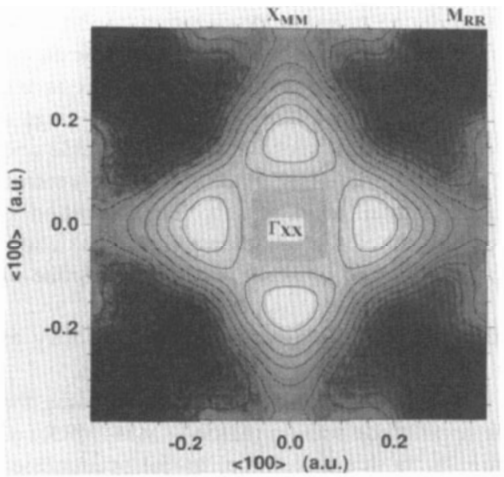

Figure 9. The experimental LCW-filtered (see the text) k-space density: the integration direction is [100]. The BZ and symmetry point notation is as in figure 2.

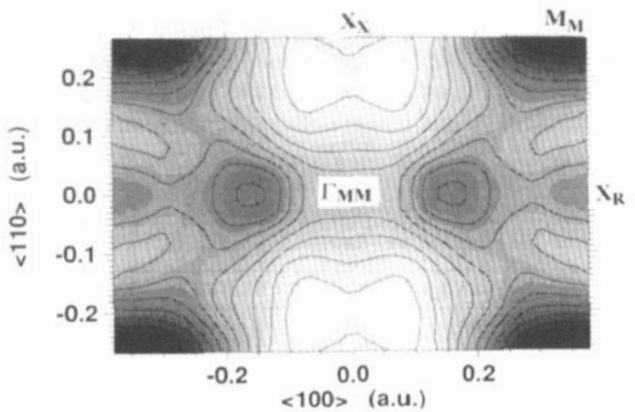

Figure 10. The experimental LCW filtered (see the text) k-space density: the integration direction is [110]. The BZ and symmetry point notation is as in figure 3.

The LCW spectra formed from the filtered momentum spectra are shown in figures 9 and 10. The improvement in the agreement between the filtered experimental data and the theory is clear: note, in particular, in the [100] spectrum (figure 9), the appearance of the predicted (figure 2) central plateau and four surrounding highs. These features are insensitive to the particular choice of smoothing parameters. We assessed, for the [100]

case, the effect of a variety of different spatial averaging masks with dimensions varying from 10 to 22 channels and obtained, in all cases, an essentially identical picture. A further test was performed on the unsymmetrized [100] projection and the patterns that emerged after filtering were, increased noise and decreased symmetry apart, consistent with those in the fully processed data. In a final test we employed the 'maximum entropy' enhancement technique described in [17]. The result was the same.

In spite of the improvement in the agreement between 2D-ACAR 'band-passed' data and the model predictions, discrepancies remain. In figure 10 (compare figure 3) these are the local slight minima at XR and XX and the fragmented highs around XX. The minima are, almost certainly, an effect of the filtering process (they are typical of the filter-induced distortions expected and encountered elsewhere [16]). The fragmentation of the high at XX is most probably (we have deduced from an examination of the band pass of the corresponding [110] LCW of the original unsymmetrized data) a manifestation of symmetrized noise. In figure 9 (compare figure 2) the major discrepancy lies in the shape of the contour lines around MRR. We can offer no explanation of this. So large a deviation from the expected ellipsoidal form of the major FS sections is inconceivable and the remaining predicted 12 small FS sections are inappropriately placed (they are centred approximately midway between Γ and M) and too small to explain it. The distortion is not typical of a filter artefact [16] and (after analysis of the unsymmetrized data) could not be related to symmetrized noise. It is conceivable but unlikely that it is a residue of wave-function effects.

Notwithstanding these residual uncertainties, we have thought it appropriate to try to estimate, from our data, the radii of the main FS ellipsoids.

We first derived a figure for the ellipsoid diameter in the square BZ face containing the X, M and R points through a simulation of the appropriate section (MRR–XMM–MRR) of the filtered LCW for the [100] projection (figure 9). In this simulation, model occupancies with ellipsoids of different minor diameter were convoluted with the experimental resolution and the diameter adjusted until the FWHM of the section matched that of the experimental data. A similar model–experiment comparison of the FWHM profile of the MM–XR–MM section of the [110] projection (figure 10) provided the same result. Finally, the ellipsoid major diameter (along the direction Γ–X in the BZ) was determined by varying the major diameter (while keeping the minor diameter at the value earlier deduced) until the model and experimental profiles were in closest accord. Table 1 lists the ellipsoid parameters deduced.

Table 1. Diameters of the FS ellipsoids of CeB_6, as percentages of the BZ size, derived as described in the text. The values are compared with the dHvA results reported in [2].

Direction	% of $2\pi/a$	Evaluated through section	dHvA: % of $2\pi/a$
X–M	65 ± 2	MR–MX–MR	68
Γ–X	75 ± 2	MX–ΓX–MX	78

As a consistency check we have computed the total (three full ellipsoids) occupied fraction of the BZ, neglecting the distortion due to the necks. The result (0.50 ± 0.03), interestingly, is much closer to the ideal 0.5 than that deduced from the dHvA results [2]. This figure is not altered by the addition of the further 0.01 for the volume of the suggested 12 small pockets along Γ–M [2].

4. Conclusions

We have performed 2D-ACAR experiments on a single crystal of CeB_6 in the paramagnetic phase for two integration directions. The 2D-ACAR distribution of the projection on the higher-symmetry [100] axis displays anisotropies consistent with the theoretical predictions of the FS. A simple and easily executed filter procedure gives final LCW results that agree reasonably well with theoretical models of the FS obtained treating the f electrons as localized. From these filtered spectra we have assessed quantitatively the main features of the FS of CeB_6, which turn out to be in good agreement with those obtained by other experimental techniques.

The success of the current analysis shows that the combination of some *a priori* knowledge of the symmetry and the topology of the Fermi surface of interest and the use of filtering procedures such as that described herein, can provide definitive information on the electronic structure of complex systems without a comprehensive and detailed calculation of the electron–positron momentum distribution.

Acknowledgments

We are indebted to N Wilkinson for technical help, to M Brand, S Dugdale and J Kaiser for their software contribution and to S Usmar for stimulating discussions. This work was supported by an SERC grant and by the financial support of the Istituto Nazionale di Fisica della Materia (INFM Italy). We gratefully thank the Ente Nazionale Energie Alternative (ENEA Italy) for allowing the temporary location of the whole detection system at the Bristol University. One of us (RNW) would like to thank the Benjamin Meaker Foundation and Bristol University for the visiting professorship which enabled his participation in this work.

References

[1] Onuki Y, Komatsubara T, Reinders P H P and Springford M 1989 *J. Phys. Soc. Japan* **58** 3698
[2] Harrison N, Meeson P, Probst P A and Springford M 1993 *J. Phys.: Condens. Matter* **5** 7435
[3] Effantin M, Rossat-Mignod J, Burlet P, Bartholin H, Kunii S and Kasuya T 1985 *J. Magn. Magn. Mater.* **47&48** 145
[4] Berko S 1983 *Positron Solid State Physics* ed W Brandt and A Dupasquier (Amsterdam: North Holland) p 64
[5] Haghighi H, Kaiser J H, Rayner S, West R N, Liu J Z, Shelton R, Howell R H, Solal F, Sterne P A and Fluss J M 1991 *Phys. Rev. Lett.* **67** 382
[6] Tanigawa S, Terakado S, Ito K, Morisue A, Komatsubara T and Onuki Y 1985 *Positron Annihilation* ed P C Jain, R M Singru and K P Gopinatan (Singapore: World Scientific) p 285
[7] Tanigawa S, Kurihara T, Osawa M, Komatsubara T and Onuki Y 1988 *Positron Annihilation* ed L Doriken-Vanpraet, M Doriken and D Seegers (Singapore: World Scientific) p 239
[8] The acquisition and coincidence electronics system was designed and assembled at ENEA Bologna by S Taiocchi, M Biasini and P Bartolomei.
[9] West R N, Mayers J and Walters P A 1981 *J. Phys. E: Sci. Instrum.* **14** 478
[10] Kubo Y and Asano S 1992 *J. Magn. Magn. Mater.* **104–7** 1182
[11] Hasegawa A and Yanase A 1977 *J. Phys. F: Met. Phys.* **7** 1245
[12] Harima H, Sakai O, Kasuya T and Yanase A 1988 *Solid State Commun.* **66** 603
[13] Matsui H, Goto T, Kunii S and Sakatsume S 1993 *Physica* B **186–8** 126
[14] Lock D G, Crisp V H C and West R N 1973 *J. Phys. F: Met. Phys.* **3** 561
[15] Jain A K 1990 *Fundamentals of Digital Imaging Processing* (Engelwood Cliffs, NJ: Prentice Hall) p 250
[16] O'Brien K M, Rayner S L and West R N to be published
[17] Dugdale S B, Alam M A, Fretwell H M, Biasini M and Wilson D 1994 *J. Phys.: Condens. Matter* **6** L435